



**HAL**  
open science

# Theoretical Investigation of the Performance of a Novel Loop Heat Pipe Solar Water Heating System for Use in Beijing, China

Xudong Zhao, Zhangyuan Wang, Qi Tang

► **To cite this version:**

Xudong Zhao, Zhangyuan Wang, Qi Tang. Theoretical Investigation of the Performance of a Novel Loop Heat Pipe Solar Water Heating System for Use in Beijing, China. *Applied Thermal Engineering*, 2010, 30 (16), pp.2526. 10.1016/j.applthermaleng.2010.07.002 . hal-00675407

**HAL Id: hal-00675407**

**<https://hal.science/hal-00675407>**

Submitted on 1 Mar 2012

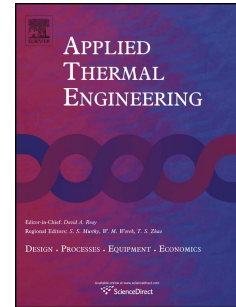
**HAL** is a multi-disciplinary open access archive for the deposit and dissemination of scientific research documents, whether they are published or not. The documents may come from teaching and research institutions in France or abroad, or from public or private research centers.

L'archive ouverte pluridisciplinaire **HAL**, est destinée au dépôt et à la diffusion de documents scientifiques de niveau recherche, publiés ou non, émanant des établissements d'enseignement et de recherche français ou étrangers, des laboratoires publics ou privés.

# Accepted Manuscript

Title: Theoretical Investigation of the Performance of a Novel Loop Heat Pipe Solar Water Heating System for Use in Beijing, China

Authors: Xudong Zhao, Zhangyuan Wang, Qi Tang



PII: S1359-4311(10)00277-2

DOI: [10.1016/j.applthermaleng.2010.07.002](https://doi.org/10.1016/j.applthermaleng.2010.07.002)

Reference: ATE 3161

To appear in: *Applied Thermal Engineering*

Received Date: 6 March 2009

Revised Date: 7 May 2010

Accepted Date: 3 July 2010

Please cite this article as: X. Zhao, Z. Wang, Q. Tang. Theoretical Investigation of the Performance of a Novel Loop Heat Pipe Solar Water Heating System for Use in Beijing, China, *Applied Thermal Engineering* (2010), doi: [10.1016/j.applthermaleng.2010.07.002](https://doi.org/10.1016/j.applthermaleng.2010.07.002)

This is a PDF file of an unedited manuscript that has been accepted for publication. As a service to our customers we are providing this early version of the manuscript. The manuscript will undergo copyediting, typesetting, and review of the resulting proof before it is published in its final form. Please note that during the production process errors may be discovered which could affect the content, and all legal disclaimers that apply to the journal pertain.

# Theoretical Investigation of the Performance of a Novel Loop Heat Pipe Solar Water Heating System for Use in Beijing, China

Xudong Zhao\*

Institute of Energy and Sustainable Development, De Montfort University, UK

Zhangyuan Wang, Qi Tang

Department of the Built Environment, University of Nottingham, UK

\* Corresponding author: tel: +44 116 257 7971; fax: +44 116 257 7981

Email: [xzhao@dmu.ac.uk](mailto:xzhao@dmu.ac.uk)

## Abstract

A novel loop heat pipe (LHP) solar water heating system for typical apartment buildings in Beijing was designed to enable effective collection of solar heat, distance transport, and efficient conversion of solar heat into hot water. Taking consideration of the heat balances occurring in various parts of the loop, such as the solar absorber, heat pipe loop, heat exchanger and storage tank, a computer model was developed to investigate the thermal performance of the system. With the specified system structure, the efficiency of the solar system was found to be a function of its operational characteristics - working temperature of the loop heat pipe, water flow rate across the heat exchanger, and external parameters, including ambient temperature, temperature of water across the exchanger and solar radiation. The relationship between the efficiency of the system and these parameters was established, analysed and discussed in detail. The study suggested that the loop heat pipe should be operated at around 72 °C and the water across the heat exchanger should be maintained at 5.1 l/min. Any variation in system structure, i.e., glazing cover and height difference between the absorber and heat exchanger, would lead to different system performance. The glazing covers could be made using either borosilicate or polycarbonate, but borosilicate is to be preferred as it performs better and achieves higher efficiency at higher temperature operation. The height difference between the absorber and heat exchanger in the design was 1.9 m which is an adequate distance causing no constraint to heat pipe heat transfer. These simulation results were validated with the primary testing results.

**Keywords:** Loop; Heat Pipe; Solar Radiation; Heat Exchanger; Hot Water; Heating

**Nomenclature**

$A$  – heat transfer (absorbing) area,  $m^2$ ;

$A_{\text{absorber}}$  – solar absorber area,  $m^2$ ;

$A_{\text{gc,eff}}$  – effective heat transfer area of outer circular glazing covers,  $m^2$ ;

$C_p$  – specific heat capacity,  $\text{kJ/kg}\cdot\text{K}$ ;

$d$  – symbol of derivative;

$D$  – diameter,  $m$ ;

$D_v$  – diameter of vapour channel in heat pipes,  $m$ ;

$g$  – gravitational acceleration,  $9.81 \text{ m/s}^2$ ;

$h$  – convective heat transfer coefficient,  $\text{W/m}^2\cdot\text{K}$ ;

$h_{\text{fg}}$  – latent heat of vaporisation,  $\text{kJ/kg}$ ;

$H$  – height,  $m$ ;

$H_f$  – frictional resistance pressure head,  $m$ ;

$H_l$  – local resistance pressure head,  $m$ ;

$I$  – solar radiation,  $\text{W/m}^2$ ;

$L$  – length,  $m$ ;

$N$  – number of heat absorbing pipes;

$Nu$  – Nusselt number;

$Pr$  – Prandtl number;

$\Delta P_{v1}$  – pressure drop from absorber to heat exchanger,  $\text{Pa}$ ;

$Q$  – heat flux,  $\text{W}$ ;

$R$  – thermal resistance,  $\text{K/W}$ ;

$Re$  – Reynold number;

$t$  – temperature, °C;

$t_{\text{tank0}}$  – initial water tank temperature, °C;

$T$  – time, s;

$\Delta T$  – time for one circulation of water across heat exchanger channels, s;

$v$  – velocity, m/s;

$\dot{V}$  – volume flow rate, m<sup>3</sup>/s;

$V$  – volume, m<sup>3</sup>;

$W$  – width, m;

$\alpha$  – absorptivity;

$\alpha_0$  – factor relating to solar collector character parameters;

$\gamma$  – absolute roughness, m;

$\delta$  – thickness, m;

$\varepsilon$  – emissivity;

$\zeta$  – frictional resistance coefficient;

$\eta$  – efficiency;

$\eta_0$  – original efficiency relating to solar collector character parameters;

$\lambda$  – thermal conductivity, W/m·K;

$\sigma$  – Stefan Boltzman constant,  $5.67 \cdot 10^{-8}$  W/m<sup>2</sup>·K<sup>4</sup>;

$\tau$  – transmittance;

$\mu$  – dynamic viscosity, Pa·s;

$\xi$  – local resistance coefficient;

$\rho$  – density, kg/m<sup>3</sup>;

$\rho_v$  – vapour density, kg/m<sup>3</sup>;

$\Phi$  – void fraction;

**Subscripts**

ab – absorber;

amb – ambient;

c – coating materials applied to the absorbers;

COP – Coefficient of Performance;

gc – glazing cover;

he – heat exchanger;

hp – heat pipe;

i – inner layer or inlet;

i, air – still air within the inner chambers;

lf – liquid film over the heat exchanger surface;

loop – heat pipe loop;

losses – heat dispersed to the ambient from the absorber;

mean – mean temperature of water flow;

o – outer layer or outlet;

p – pores in wicks;

pump – circulation pump;

rad – radiative heat transfer within vacuum space between two circular glazing covers;

sw – surface wall;

tank – water storage tank;

vh – vapour header;

vl – vapour line;

w – water flow;

wb – wall board in south façade of building;

wf – working fluid;

wi – wicks;

wp – water pipe between the heat exchanger and storage tank;

## 1. Introduction

Over past decades, solar water heating systems have become common practice in housing stock worldwide [1, 2, 3, 4]. Most solar water heaters for buildings are flat-plate types or conventional heat pipe arrays which are usually installed on roofs for layout convenience. This type of installation requires long runs of piping delivering water from the roof heaters to the working points and receiving water from the water mains. The cost of the system is therefore high and most importantly, the installation detracts the aesthetic view of the building, particularly those multi-storey buildings with numerous users, as well as the whole city (or district) landscape.

In recent years, several building façades based solar heaters have appeared on the market and been used in practical projects [5]. These devices are positioned on walls or balconies, avoiding the requirement for roof space and shortening the distance of pipe runs, and therefore increasing the building's aesthetic view. However, these devices still require the transportation of water from inside of the building to the outside, which may subject to the hazard of pipe freezing during winter operation.

Loop heat pipes (LHPs) are two-phase heat-transfer devices separating the vapour and liquid flows and eliminating the entrainment effect between them, which is one of the major limits for heat pipe heat transfer. They are therefore able to transfer large amounts of heat for distances up to several metres, or to several tens of metres in a horizontal (vertical) position through the effect of capillary pumping or gravity [6, 7]. Due to this feature the loop heat pipes are ideally suited for use in building hot water systems, which allow solar heat to be collected from an outer façade area, transported to a heat exchanger at the inside of the building, and further transferred to the water flowing across the exchanger. This will prevent long distance running of the water from the inside of the building to outside, and thus protect water pipes from freezing during winter operation. It

should be emphasized that the liquid within the loop is an anti-freezing fluid, i.e., water/glycol mixture, which is separated from the water to be heated, and therefore has no effect on the quality of water for living and causes no harm to users. This type of liquid possesses unique characteristics [7, 8], namely high latent heat, and adequate boiling temperature as well as good compatibility with heat pipe materials (copper and aluminium) and is, therefore, an ideal choice for heat pipe operation.

In this paper, a prototype loop heat pipe system for a Beijing apartment building hot water supply was designed. By adopting the heat balance and thermal resistance network method, a computer model was developed to simulate the heat transfer processes across various parts of the system. Simulation results obtained from running the model were used to estimate the system's efficiency ( $\eta$ ) and determine the relationship between the efficiency ( $\eta$ ) and various parameters relating to the system structure and operating conditions. For validation, the simulation results were compared with the testing results.

## 2. System description

The schematic of the proposed system is shown in Figure 1. The system, filled with an anti-freezing working fluid, is composed of wicked heat absorbing pipe arrays, vapour and liquid headers, vapour and liquid transporting lines, as well as a flat-plate heat exchanger coupled with a water storage tank by water tubing. The absorbing pipes are attached with fins and, outside of the pipes, are fitted with the double skin, evacuated glass covers. The glass-attained pipes are tightly arranged in parallel with a very small gap in between and attached vertically to the south facing wall of the building, which could be made of reinforced polystyrene. This installation allowed maximum solar absorption by the pipes and minimum heat losses occurred from the pipes to the surroundings. It should be addressed that the liquid within the heat pipe was a mixture of water and glycol [9]. However, since small amount of glycol (< 5% of total volume of the heat pipe loop) was added into the system, its influence to system heat transfer was minor. In this theoretical analysis, liquid within the pipe was treated as pure water, while the existence of glycol was ignored.

In operation, the received solar heat converts the liquid adhered on the wick of the pipes into vapour, which flows upwards along the inner space of the pipes and enters the top-side vapour header, owing to the buoyancy of vapour. The vapour is further transported to the heat exchanger inside the building via the vapour transporting line. Within the exchanger, the vapour is condensed into liquid of the same temperature, transferring heat to the water flowing across the channels adjacent to the vapour channels. At the outlet of the exchanger, a steam trap is assembled to stop penetration of vapour through the pipe. Thus, only the condensed liquid can flow across and enter the liquid transporting line. Via the line, the liquid enters the liquid header located right below the vapour header, due to the gravity caused by the height difference between the exchanger and the header. This amount of liquid is then evenly distributed to individual pipes through a dedicated liquid feeder fitted at the upper part of the pipes, as shown in Figure 2. The feeder is a cylinder structure with round-distributed mini-holes with 1 mm of diameter at the bottom, which would allow the liquid to be dipped into the wick voids equally. The speed of liquid feeding can be controlled by adjusting the height level of the liquid within the feeder in order to achieve a balance between liquid evaporation and supply, which could be ‘tasted’ through a specially designed sensor installed on position. Thus, the liquid adhered within the wick can be evaporated instantly with little accumulation or not at the bottom of the pipes, which helps maximise heat transfer occurring in the pipes.

This loop heat pipe system removes the need to transport water for a long distance, i.e., from inside to outside, and then back to inside of the building. Instead, the water, raised by a pump, simply circulates around the exchanger channels to obtain heat from the vapour and back into the water-storage right beside the exchanger. The heated water will then be delivered to working points when needed.

The absorber area could be suitably sized to meet hot water demand for the targeted house, depending upon the system’s solar efficiency and number of occupants served. For a typical 3-member family flat in Beijing (China), the initial size of the absorber is chosen as 3 m<sup>2</sup> and its average solar efficiency is assumed to be 60%. This would allow sufficient heat to be obtained

from the sun to raise about 198 litres of water, including shower (97.2 litres), laundry (25.65 litres), cooking (75 litres), from its initial temperature (around 10 °C) to working temperature (40 °C) during the day-time period [10]. This amount of water will then be used in the afternoon and evening when people are back home. Other components of the system were also sized accordingly. It should be stressed that all above figures are primarily set and will be subject to further adjusting and variation, depending upon the results of simulation. Two types of glass tubes, borosilicate and polycarbonate, were considered and their thermal and physical properties were presented in Table 1 [11, 12]. The heat absorbing pipes are made of copper and their thermal and geometrical parameters were given in Table 2 [13, 14, 15]. Other system components including vapour/liquid headers and lines, as well as water pipes between heat exchanger and storage, were also specified, as shown in Table 3. Finally, Table 4 presented the technical specifications of the heat exchanger selected [14, 16].

### 3. Mathematical analysis of the thermal process and computer model set-up

Heat transfer occurring in the LHP system involves three major processes, i.e., conversion of solar radiation into heat received by the absorbers, transporting of the absorbed heat from the absorbers to the heat exchanger via evaporation and condensation of the heat pipe working fluid, as well as transferring the heat from exchanger to the passing water. These processes are inter-linked and will finally achieve a balance under the steady state operation, and could be illustrated as follows:

#### 3.1 Conversion of solar radiation into heat received by the absorber

The solar energy entering the inner chamber of the pipe arrays across the double skinned and evacuated glasses and absorbed by the coating materials attached on the absorbers,  $Q_c$ , could be expressed as follows [17]:

$$Q_c = \tau_{gc,o} \tau_{gc,i} \alpha_c A_{gc,eff} I = \tau_{gc,o} \tau_{gc,i} \alpha_c A_{gc,o} N_{gc,o} I \quad (1)$$

This part of the heat is partly absorbed by the finned pipes and the remainder is dispersed to the atmosphere due to temperature difference between the absorber surface and ambient air, which is illustrated in Figure 3.

For an absorber surface with temperature of  $t_{ab,sw}$ , the heat dispersion could be written as [18]

$$Q_{losses} = \frac{t_{ab,sw} - t_{amb}}{R_{amb} + R_{gc,o} + R_{rad} + R_{gc,i} + R_{i,air}} \quad (2)$$

$$R_{amb} = \frac{1}{h_{amb}} \frac{1}{A_{gc,o}} \frac{1}{N_{gc,o}} \quad (3)$$

$$R_{gc,o} = \frac{\delta_{gc,o}}{\lambda_{gc,o}} \frac{1}{A_{gc,o}} \frac{1}{N_{gc,o}} \quad (4)$$

$$R_{rad} = \frac{\frac{1}{\varepsilon_{gc,o}} + \frac{1}{\varepsilon_{gc,i}} - 1}{\sigma(t_{gc,o} + t_{gc,i})(t_{gc,o}^2 + t_{gc,i}^2)} \frac{1}{\frac{A_{gc,o} + A_{gc,i}}{2}} \frac{1}{N_{gc,i}} \quad (5)$$

$$R_{gc,i} = \frac{\delta_{gc,i}}{\lambda_{gc,i}} \frac{1}{A_{gc,i}} \frac{1}{N_{gc,i}} \quad (6)$$

$$R_{i,air} = \frac{1}{h_{i,air}} \frac{1}{A_{gc,i}} \frac{1}{N_{gc,i}} \quad (7)$$

The heat absorbed by the absorbing surface is

$$Q_{ab} = Q_c - Q_{losses} \quad (8)$$

### 3.2 Transporting of the absorbed heat from the absorbers to the heat exchanger

The absorbed heat ( $Q_{ab}$ ) should be immediately taken away from the absorbers by using the heat pipe loop. This could be achieved by liquid evaporation in absorbing section and vapour condensation in the heat exchanger surface. This part of heat could be written as [13, 17, 18]

$$Q_{loop} = \frac{t_{ab,sw} - t_{he,sw}}{R_{hp,sw} + R_{wi} + R_{vl} + R_{lf} + R_{he,sw}} \quad (9)$$

This process involves several thermal resistances, as indicated in Figure 4. These resistances are the key factors impacting on magnitude of heat transfer and could be illustrated separately as follows.

Absorbing pipe wall resistance:

$$R_{hp,sw} = \frac{\ln(D_{hp,o}/D_{hp,i})}{2\pi L_{hp}\lambda_{hp}} \frac{1}{N_{hp}} \quad (10)$$

Saturated wicks resistance:

$$R_{wi} = \frac{\ln(D_{hp,i}/D_v)}{2\pi L_{wi}\lambda_{wi}} \frac{1}{N_{hp}} \quad (11)$$

Where  $\lambda_{wi}$  was the effective thermal conductivity of the wicks which has taken into account porosity of wicks [18].

Vapour flow resistance:

$$R_{vl} = \frac{t_{loop} \times \Delta P_{vl}}{\rho_v \times \rho_{wf} \times \dot{V}_{wf} \times h_{fg}^2} \quad (12)$$

The vapour will flow across three regions in sequence, i.e., absorbing piping, transporting piping and heat exchanger channels. The volume flow rate of the vapour could be expressed as

$$\dot{V}_{wf} = \frac{Q_{ab}}{\rho_{wf} \times h_{fg}} \quad (13)$$

In operation, the vapour will not fully possess the loop space and therefore, a parameter called vapour void fraction is defined as follows [18]:

$$\Phi = \frac{T \times \dot{V}_{wf}}{\pi(D/2)^2 L} \quad (14)$$

The vapour will withstand several pressure drops when flowing across these different regions of the loop, which could be expressed as follows [18]:

For the heat absorbing pipes:

$$\Delta P_{vl, hp} = \frac{\dot{V}_{wf} \times \rho_{wf}}{8 \rho_v (D_v/2)^4} \frac{1}{N_{hp}} \quad (15)$$

Since the heat absorbing pipes are parallel arranged, the full vapour flow will be divided into numerous vapour streams that will be equally distributed into the individual pipes, the pressure losses across the absorbing pipes are therefore adversely affected by the number of the heat absorbing pipes.

For the vapour header and vapour transporting line,

$$\Delta P_{vl, vh \text{ or } vl} = \frac{8 \mu_{wf} L}{\pi \rho_v (D/2)^4} \quad (16)$$

For the heat exchanger channels (vapour region):

$$\Delta P_{vl, he} = - \frac{4}{\pi^2} \frac{\dot{V}_{wf} \times \rho_{wf}}{8 \rho_v (D_{he,i}/2)^4} \frac{1}{(\frac{N_{he}}{2} - 1)} \quad (17)$$

The total vapour pressure drop across the loop is

$$\Delta P_{vl} = \Delta P_{vl, hp} + \Delta P_{vl, vh} + \Delta P_{vl, vl} + \Delta P_{vl, he} \quad (18)$$

The condensed liquid film will be evenly distributed across the exchanger surfaces at the heat pipe fluid side and its associated flow resistance is:

$$R_{lf} = \frac{\ln(D_{he,i}/(D_{he,i} - 2\delta_{lf}))}{2\pi L_{lf} \lambda_{lf}} \frac{1}{(\frac{N_{he}}{2} - 1)} \quad (19)$$

Heat exchanger wall resistance:

$$R_{he, sw} = \frac{\ln(D_{he,o}/D_{he,i})}{2\pi L_{he} \lambda_{he}} \frac{1}{(\frac{N_{he}}{2} - 1)} \quad (20)$$

As the vapour and liquid transporting lines are fully insulated, there will be very little heat losses across the piping surfaces and therefore, the heat losses through the transporting lines to surroundings could be ignored.

It should be addressed that prior to calculating heat pipe heat transfer, the limit of heat transport capacity of the loop pipe system should be examined. The limit of heat transport capacity means the maximum heat transfer the system can take, which would occur at the condition that the system's driving force, i.e., gravity or capillary, matches with the overall flow resistance [17, 19]. Running an established computer programme yields the limit of the heat transport capacity of the system when the height difference between the absorber and heat exchanger is 1.9 m, i.e., 1806 W/m<sup>2</sup>, which is larger than the maximum available solar energy striking on the south-facing facade at Beijing, i.e., 855 W/m<sup>2</sup> [20]. Therefore, the loop heat pipe system has sufficient capability to transport the heat from solar irradiance with no restriction from its own structure.

### 3.3 Transferring the heat from heat exchanger to the passing water

The heat transferred to the exchanger surface will be taken away by the passing water, thus resulting in an increase of water temperature, which is shown in Figure 5. A long period of operation, such as 8-hour day-time, would result in a continuous rise of water temperature and allow the required household water temperature to be achieved.

For an inlet water temperature  $t_i$ , a temperature rise ( $t_o - t_i$ ) is expected after the water passes across the exchanger. The heat transfer between the exchanger surface and the passing water could be expressed as [18]:

$$Q_{he} = \frac{A_{he} \times \left( t_{he,sw} - \frac{(t_i + t_o)}{2} \right)}{\frac{1}{h_w}} = C_p \dot{V}_w \rho_w (t_o - t_i) = Q_{loop} \quad (21)$$

Where  $\dot{V}_w$  is the water volume rate maintained by the pump and  $h_w$  is the water convective heat transfer coefficient and could be illustrated as follows:

For the water flowing across a single heat exchanger channel,

$$h_w = \frac{Nu * \lambda_w}{D_{he,o}} \quad (22)$$

As water will flow across the exchanger channels at relatively low speed, the flow could be treated as laminar. In this case, the Nusselt number, Nu, could be written as follow:

$$\text{Nu} = 1.86 \text{Re}^{\frac{1}{3}} \text{Pr}^{\frac{1}{3}} \left( \frac{D_{\text{he},o}}{L_{\text{he}}} \right)^{\frac{1}{3}} \left( \frac{\mu}{\mu_{\text{he},sw}} \right)^{0.14} \quad (23)$$

Of which, Reynolds number (Re) and Prandtl number (Pr) could be expressed as follows:

$$\text{Re} = \frac{v_w * D_{\text{he},o} * \rho_w}{\mu_w} \quad (24)$$

$$\text{Pr} = \frac{C_p * \mu_w}{\lambda_w} \quad (25)$$

$(\mu/\mu_{\text{he},sw})^{0.14}$  is the factor in relation to the exchanger plate temperature and could be treated as 1.05 at heating operation status [18].

It should be understood that when the water receives the thermal energy from the sun through the LHP system, it, in the meantime, also consumes a certain amount of electrical energy due to operation of the circulation pump. This part of electrical energy will be used to overcome the flow resistance across the water cycle between the water storage and heat exchanger, including frictional resistance and local fitting resistance, and keep an adequate water circulation rate. The hot water pump power could be calculated as follows [18]:

In this system, frictional resistance losses refer to pressure losses across the straight connection pipe lines between the heat exchanger and water storage tank. The friction factor associated with the losses could be determined and calculated using the following equations:

$$\text{If } \text{Re} \leq 2000, \quad \zeta = \frac{64}{\text{Re}} \quad (26)$$

$$\text{If } \text{Re} > 2000, \quad \zeta = \frac{1}{\left[ 1.14 - 2 \log_{10} \left( \frac{\nu}{D} \right) \right]^2} \quad (27)$$

$$H_f = \sum \zeta \frac{L}{D} \frac{v_w^2}{2g} \quad (28)$$

Local resistance losses refer to the pressure drops occurred at the local fittings assembled in the system, including 2 valves, 6 sudden expansions/contractions and 2 bends. The local resistance factor,  $\xi$ , for each fitting could be obtained from ref. [21]. Thus the total local resistance pressure losses could be expressed as:

$$H_l = \sum \xi \frac{v_w^2}{2g} \quad (29)$$

The power consumption occurred in the water cycle could be expressed as:

$$Q_{\text{pump}} = \frac{\dot{V}_w \rho_w g (H_f + H_l)}{\eta_{\text{pump}}} \quad (30)$$

The coefficient of performance (COP) of the system could be defined as the ratio of collected heat and pump power, as follows [22]:

$$\text{COP} = \frac{Q_{\text{he}}}{Q_{\text{pump}}} \quad (31)$$

### 3.4 Computer modelling set-up

The three heat transfer processes will finally achieve a balance when the system operates at the steady state condition and each section of the system remains a certain temperature. The algorithm used for the modelling set-up is indicated as follows:

- 1) Given a LHP system structure, the parameters related to the system configuration could be obtained, which are shown in Table 1, Table 2, Table 3 and Table 4;
- 2) Given the operating temperature of the heat pipe system, the thermodynamic parameters of the working fluids could be obtained;
- 3) Assuming the external conditions (solar radiation and ambient temperature) and inlet water temperature and water flow rate across the changer channels;
- 4) Assuming an absorber temperature  $t_{\text{ab,sw}}$ , heat analysis is carried out as follows:
  - Heat balance of the glazing cover could be analysed, which will result in the determination of the glazing surface temperature;

- Heat balance of the absorber pipes (evaporator) could be analysed using Equations (1) to (8), which will result in determination of the absorber heat gain,  $Q_{ab}$ .
  - Heat balance of heat pipes and heat exchanger pair could be analysed using Equations (9) to (25), which will result in determination of the heat gain of the water passing through the heat exchanger,  $Q_{he}$ , and outlet hot water temperature,  $t_o$ .
- 5) If  $(Q_{ab} - Q_{he})/Q_{ab} > 0.5\%$  (error allowance), then increase  $t_{ab,sw}$  by  $0.1\text{ }^{\circ}\text{C}$ , and return to step 4 for re-calculation.
  - 6) If  $(Q_{ab} - Q_{he})/Q_{ab} < -0.5\%$  (error allowance), then decrease  $t_{ab,sw}$  by  $0.1\text{ }^{\circ}\text{C}$ , and return to step 4 for re-calculation.
  - 7) If  $-0.5\% \leq (Q_{ab} - Q_{he})/Q_{ab} \leq 0.5\%$ , heat balance in the whole system is achieved.
  - 8) Energy consumed by pump,  $Q_{pump}$ , could be analysed using Equations (26) to (30).
  - 9) System performance COP can be obtained by using Equation (31).
  - 10) Program stops.

#### 4. Results and discussions

Results obtained from the simulations are used to calculate the efficiency of the system,  $\eta$ , which is defined as the ratio of heat taken away from heat exchanger by the water, and the solar radiation striking on the solar absorber [13, 18]. The efficiency should be a parameter in relation to external conditions, i.e., solar radiation, ambient temperature and temperature of water across the exchanger, its own operating characteristics, i.e., heat pipe operating temperature, water flow rate across the exchanger, as well as its structure parameters, i.e., materials for double glazing covers, height difference between heat exchanger and absorber. The relations between the efficiency and above parameters are illustrated as below:

##### 4.1 Efficiency .vs. external parameters

Under certain system structure/configuration (with borosilicate glazing as the covers) with thermal/geometric data shown in Table 1, 2, 3 and 4, and a fixed heat pipe operating temperature of  $60\text{ }^{\circ}\text{C}$  (by pre-set vacuum) and water flow rate across the exchanger channels of  $8.3\text{ l/min}$ , the solar efficiency of the system,  $\eta$ , would vary solely with the external parameters, i.e., solar radiation  $I$ , ambient temperature  $t_{amb}$ , as well as the mean temperature of water across the exchanger channels

$t_{\text{mean}}$ . These parameters are usually grouped into a specially-defined parameter, termed,  $(t_{\text{mean}}-t_{\text{amb}})/I$ . In that case,  $\eta$  may be expressed as the function of  $(t_{\text{mean}}-t_{\text{amb}})/I$ , as follows:

$$\eta = \eta_0 + \alpha_0 \left( \frac{t_{\text{mean}}-t_{\text{amb}}}{I} \right) \quad (32)$$

The data for solar radiation, ambient temperature and initial inlet water temperature were summarised in Table 5, which took the monthly average values of Beijing as the index [23]. Running the above computer model yielded the results of outlet water temperature, which was then used to develop the relationship between efficiency and  $(t_{\text{mean}}-t_{\text{amb}})/I$ .

The results of the simulation were presented in Table 6 as well. These data could also be plotted in an excel chart and relation between  $\eta$  and  $(t_{\text{mean}}-t_{\text{amb}})/I$  could be presented in a linear equation, as shown in Figure 6. It was found that under certain level of solar radiation and ambient temperature, higher water temperature will result in lower system efficiency. Having fixed up water and ambient temperature, the efficiency will increase with the solar radiation increasing. Under certain solar radiation and water temperature, the efficiency will increase when the ambient temperature increases.

#### 4.2 Impact of heat pipe operating temperature

It should be understood that the vacuum level during the manufacturing process controls the boiling (saturation) point of the working fluid. In the meantime, the solar radiation striking on the surface of the absorber, the ambient temperature and the temperature and flow rate of the water, the combined effect of these five parameters would result in the heat pipe operating temperature.

Remaining system physical (structure) condition, external condition and water flow rate same as in Section 4.1, but leaving the vacuum inside the heat pipe changes accordingly, causing the heat pipe operating temperature free to change from 40 °C to 75 °C, the efficiency of the solar system was investigated by running the established program and the results were shown in Figure 7. It was found the efficiency kept trend of increase with the temperature increasing till 72 °C, but further increase in heat pipe operating temperature would result in a rapid decline in system efficiency.

The reason for this could be briefly illustrated as follows: high heat pipe operating temperature would benefit heat transfer between the heat pipe working fluid and the passing water, while in the mean time causing increased heat losses from the heat absorber to the surroundings. There would be a balance point in existence that could allow the highest solar efficiency (63% for this case) to be achieved and this balance point would represent a proper operating temperature, which is 72 °C under this case study.

#### **4.3 Impact of water flow rate**

Theoretically, high water flow rate would lead to enhanced convective heat transfer between the heat pipe condensing fluid on one side of the heat exchanging plate and water flow across the other side and therefore, enhanced heat output in terms of solar energy conversion. However, high water flow rate would also lead to increased pump power. In this case, the system heat output and COP would be two parallel items used to justify the optimum water rate across the exchanger. Remaining the solar system structure and operating parameters same as the above, variation of the heat output and system COP against water flow rate across the exchanger were simulated and the results are shown in Figure 8. It was found the system heat output increased gradually but its COP decreased significantly when water flow rate increased. Therefore, there would be an appropriate rate in existence that would remain both system heat output and COP high. A comparative analysis indicated that the water flow rate across the heat exchanger should be around 5.1 l/min, which is controllable through adjusting the motor speed and valves.

#### **4.4 Impact of absorber glazing covers**

Under certain system operating conditions, i.e., weather and water parameters, the efficiency of the solar system would depend upon its own structure, particularly type of the top glazing cover. Ideally the glazing should allow maximum solar irradiance to be transmitted and also be able to minimise heat losses from the absorber to ambient. Double-skinned polycarbonate and borosilicate are potential materials for this use due to their higher solar transmittances and lower U values.

Remaining the above system structure and operating conditions same, its efficiencies for two top glazing covers operation were simulated and the results are illustrated in Figure 9. It indicates that borosilicate cover is able to achieve higher efficiency than polycarbonate does at higher temperature operation, i.e.,  $t_{\text{mean}} > t_{\text{amb}}$ , while the polycarbonate is suitable for low water temperature ( $t_{\text{mean}} < t_{\text{amb}}$ ). The reason is that the borosilicate has higher solar transmittance which helps receiving larger solar irradiance. However, its U value is larger that would increase heat transfer between ambient and passing water, thus leading to lower efficiency under low temperature operation.

The final choice for the top cover is borosilicate as it could retain thermal performance for long periods of operation. Polycarbonate would experience faster degradation, in terms of the thermal properties including absorptivity, emissivity and transmittance, which is unsuitable for long term use in a solar system.

#### **4.5 Impact of the height difference between solar absorber and heat exchanger**

As the loop system is driven by gravity, the height difference between the top solar absorber and heat exchanger plays a key role in terms of its heat transfer capacity (limit). In operation, gravity should be larger than the flow resistance of the working fluid across the loop cycle, which is the major condition enabling operation of the system. However, keeping increase on heat input would lead to consistent increase of flow resistance, which would eventually reach the available gravity. At this point the system would achieve its maximum heat transfer and no further heat could be added up. This amount of heat is defined as the limit (or capacity) of the LHP heat transfer. The variation of heat transfer capacity (limit) against height difference between solar absorber (top level) and heat exchanger (centre level) was simulated using the previously established program and the results are shown in Figure 10. As the maximum solar radiation of Beijing in south facing orientation is  $855 \text{ W/m}^2$ , whilst the heat transport capacity (limit) of the system at 0.4 m height difference is  $878 \text{ W/m}^2$ , the system should have sufficient capability transporting heat striking on absorbing surface under the height difference between the absorber and the heat exchanger larger than 0.4 m. For the current system with 1.9 m height difference, it should be no problem at all to transfer the solar heat while causing no constraint from its structure.

#### 4.6 Validation of the simulation results using the primary testing results

A prototype system was constructed and tested in SRB (Sustainable Research Building) lab, University of Nottingham. The photograph of the prototype and the associated testing rig is presented in Figure 11. The absorbing pipes are enclosed by the double glazed, evacuated tubes, attached to the polystyrene insulation board, and connected to the liquid/vapour headers. The headers are linked to the heat exchanger located at the upper (0.5 m above) and left (2 m away) side of the absorbing pipes using the insulated connection pipes, thus forming a heat pipe loop. The connection pipes are about 2.5 meter long with incorporation of a number of bends, valves and a steam trap. The exchanger is also linked to a water storage tank, which is located at 1 m below the exchanger using a short pipe circuit incorporating the insulated pipelines, a pump, a water flow meter and 2 valves, thus forming the water cycle to prepare the hot water for the occupants' use. At the end of vapour and liquid transporting lines, and the inlet and outlet of the water pipes, as well as the side wall of the water tank (referred to Figure 12), T-type thermocouple probes were installed to measure the temperatures of the fluids. A pressure transducer with accuracy of 1% was also installed at the vapour transporting line to measure the heat pipe operating pressure. All these measurement sensors were linked to a DT500 data logger and a computer for data recording and analyses.

The testing ran for 8 hours (between 9:00 am to 5:00 pm) and the data were recorded every 1 second. The testing was carried out on a fixed solar radiation of  $816 \text{ W/m}^2$  in accordance to the maximum solar radiation at south direction in Beijing, China, an ambient temperature of  $22 \text{ }^\circ\text{C}$ , and an optimized water flow rate of 1.6 l/min. It should be noted that due to the limitation of budget, the system were built smaller than the original design. The geometric and thermal properties of the prototype testing system are detailed in Table 6.

Figure 12 shows the trend of variation of the circulation water temperature and loop heat pipe operation temperature over the measurement duration. The loop het pipe operating temperature rose rapidly at the start-up stage (about 20 minutes) and remained fairly constant afterwards. The inlet/outlet and tank water temperatures grew constantly all the time whereas the ambient

temperature remained about the same. It was found that there were large fluctuations in the heat pipe operating temperature and water flow outlet temperature during the measurement which was caused by setting of thermocouple probes. The probes were intruded into the narrow water (vapour) flow tunnels, creating turbulence of water flow around the probes and eventually effecting on stability of temperature measurement. To smooth the problem, some odd measurement data that are obviously incorrect were removed from the database. In the meantime, an appropriate data treatment was conducted: the average values of measurement data in 3 minutes intervals were calculated and implemented into the database, thus forming a diagram (Fig. 12) which could show the true trend of variation of temperature over the testing period.

Using the moving average method, i.e., taking the average values of the measured parameters within a certain time interval (12 minutes), the relation between solar efficiency and  $(t_{\text{mean}}-t_{\text{amb}})/I$  were obtained, as shown in Figure 13. A trend-line showing efficiency decreasing with  $(t_{\text{mean}}-t_{\text{amb}})/I$  increasing was clearly presented, but certain level of scattering appeared on the diagram, due to slow thermal response of the system. The testing efficiency was about 10% lower than the theoretical efficiency due to various possible reasons, e.g., heat losses occurred in the vapour/liquid transporting lines, less than expected heat transfer rate within the flat plate heat exchanger, as well as some simplifications made in the model set-up.

It should be noted that due to limitation of lab condition, it is unlikely to imitate the actual operation of the system under real climate condition. However, the efficiency figures generated from the lab testing are able to be put into comparison with those derived from the computer simulation. The difference between the theoretical and testing efficiencies was found under the reasonable error limit. The comparison could be used to analyse the accuracy of the computer program, as well as verify the effectiveness of the system

## 5. Conclusions

This paper introduced a novel loop heat pipe solar water heating system suitable for use in typical Beijing apartment buildings, which comprises a facade integrated solar absorber, heat pipe loop, heat exchanger and associated hot water tank and water cycle system. A computer model was

developed and used to analyse performance and operating characteristics of the system. The major findings could be outlined as below:

Solar efficiency of the system varies linearly with the defined parameter,  $(t_{\text{mean}}-t_{\text{amb}})/I$ , which represents the combined effect of weather and water conditions. The system efficiency increases with increasing of ambient temperature and solar radiation, but decreases with increasing of the mean temperature of water flow.

The optimum heat pipe operating temperature is around 72 °C, which would allow the maximum system solar efficiency to be achieved.

When water flow rate across the heat exchanger increases, the system heat output increases gradually and its COP is decreased significantly. An appropriate water flow rate would maintain both system heat output and COP high. A comparative analysis suggested that the water flow rate should be around 5.1 l/min.

A borosilicate cover is able to achieve higher efficiency than polycarbonate does at higher water temperature operation; whereas the polycarbonate is suitable for low water temperature. However, the final choice of top cover material is borosilicate which has more durable thermal performance and is suitable for long term operation of the solar system.

The loop heat pipe system is able to transfer received solar heat completely without constraint from its heat transport limit, even at 0.4 metre height difference between the top of the absorber and mid level of the exchanger. This system has 1.9 m of height difference which is sufficient to conduct the required heat transfer.

A prototype was constructed and tested and the experimental results were compared with the theoretical data. This comparison indicated that the system could operate effectively in lab condition but its efficiency is slightly lower than the theoretically predicted data due to a number of reasons, e.g., heat losses occurred in the vapour/liquid transporting lines, less than expected heat

transfer rate within the flat plate heat exchanger, as well as some simplifications made in the model set-up.

## Reference

- [1] H. Li, H. Yang, Potential Application of Solar Thermal Systems for Hot Water Production in Hong Kong, *Applied Energy* 86 (2009) 175-180.
- [2] A. Shukla, D. Buddhi, et al, Solar Water Heaters with Phase Change Material Thermal Energy Storage Medium: A Review, *Renewable and Sustainable Energy Reviews* 13 (2009) 2119-2125.
- [3] X.Q. Zhai, R.Z. Wang, Experience on Solar Heating and Cooling in China, *Renewable and Sustainable Energy Reviews* 12 (2008) 1110-1128.
- [4] D. Jaehnig, C. Isaksson, Solar Integration, Five Easy Ways to Incorporate Solar Thermal into Conventional Heating Systems, *Renewable Energy World* 6 (2006) 66-72.
- [5] M. Yoshikawa, Solar Heat Collector System, United State Patent, Patent number: 4901537, Date of patent: 20 Feb 1990.
- [6] S. Launay, V. Sartre, J. Bonyour, Parametric Analysis of Loop Heat Pipe Operation: a Literature Review, *International Journal of Thermal Science* 45 (2007) 621-636.
- [7] D. Reay, P. Kew, *Heat Pipe*, five ed., Elsevier, 2006, 48-52, 93-96, 122 and 234-236.
- [8] M. Groll, M. Schneider, V. Sartre, M.C. Zaghoudi, M. Lallemand, Thermal Control of Electronic Equipment by Heat Pipes, *Revue Générale de Thermique* 37 (1998) 323-352.
- [9] <<http://www.engineeringtoolbox.com/>>
- [10] China Construction Ministry, the Standard of Water Quantity for City's Residential Use, GB/T 50331-2002, China Building Industry Press, Beijing, China, 2002.
- [11] <<http://www.schott.com/>>
- [12] <<http://www.bondor.co.nz/>>
- [13] S.B. Riffat, X. Zhao, P.S. Doherty, Developing a Theoretical Model to Investigate Thermal Performance of a Thin Membrane Heat-pipe Solar Collector, *Applied Thermal Engineering* 25 (2005) 899-915.
- [14] CIBSE Guide A, Environmental Design, Page Bros. (Norwich) Ltd., Norwich, UK, 1999, 3-44.

- [15] A. Faghri, Heat Pipe Science and Technology, one ed., Taylor & Francis Group, 1995, 130-132.
- [16] <<http://www.swep.net/>>
- [17] X. Zhao, Investigation of a Novel Heat Pipe Solar Collector/CHP System, University of Nottingham, Ph.D. Thesis, 2003, 102-114.
- [18] U.S. Department of Energy, DOE Fundamentals Handbook: Thermodynamics, Heat Transfer, and Fluid Flow, Washington D.C., 1992.
- [19] S.B. Riffat, X. Zhao, P.S. Doherty, Analytical and Numerical Simulation of the Thermal Performance of 'mini' Gravitational and 'micro' Gravitational Heat Pipes, Applied Thermal Engineering 22 (2002) 1047-1068.
- [20] China Construction Ministry, Code for Design of Heating, Ventilation and Air Conditioning, GB 50019-2003, China Planning Press, Beijing, China, 2003, 110-112.
- [21] CIBSE Guide C: Reference Data, Page Bros (Norwich) Ltd., Norwich, UK, 2001, 100-140.
- [22] C.H. Blanchard, Coefficient of Performance for Finite Speed Heat Pump, Journal of Applied Physics 51(1980) 2471-2472.

## Figures and Tables

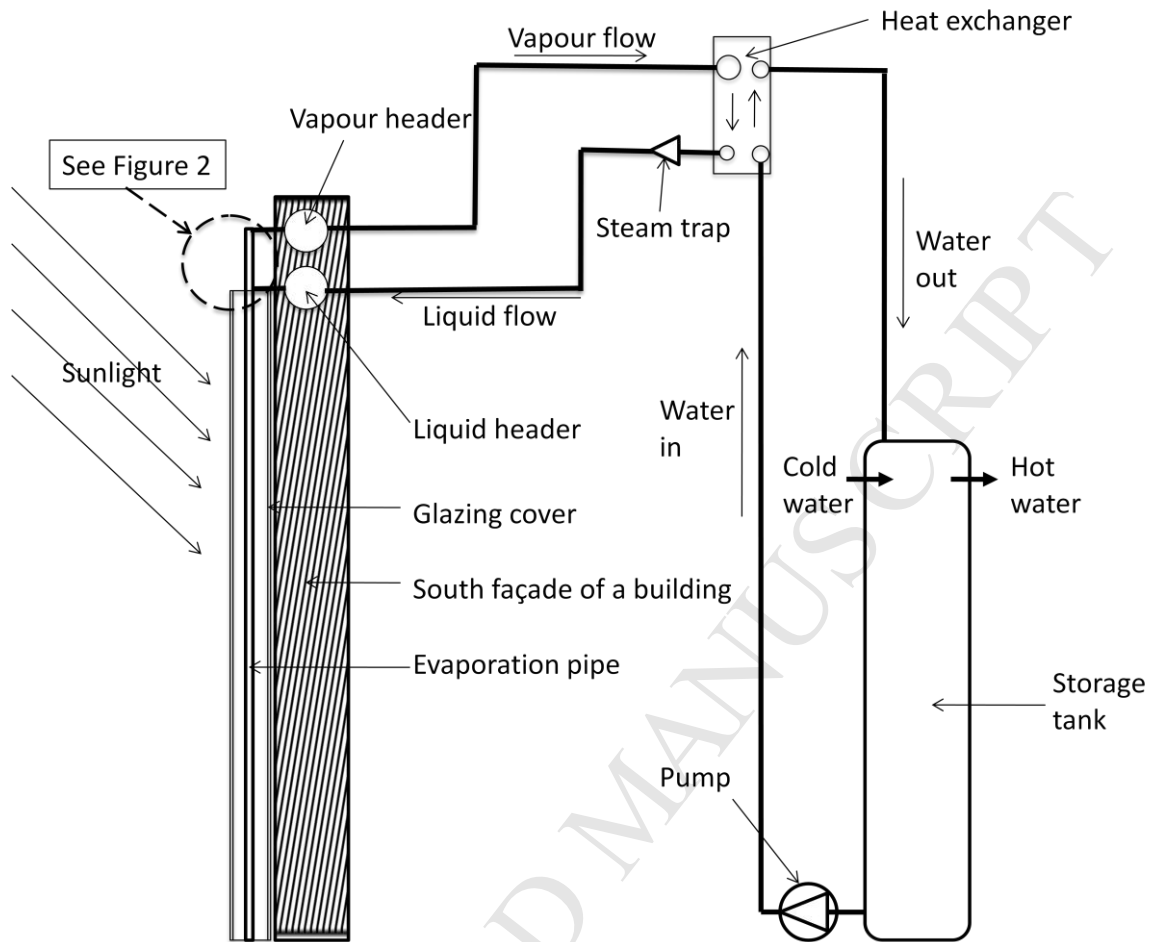


Fig. 1. Schematic of the LHP solar hot water heating system

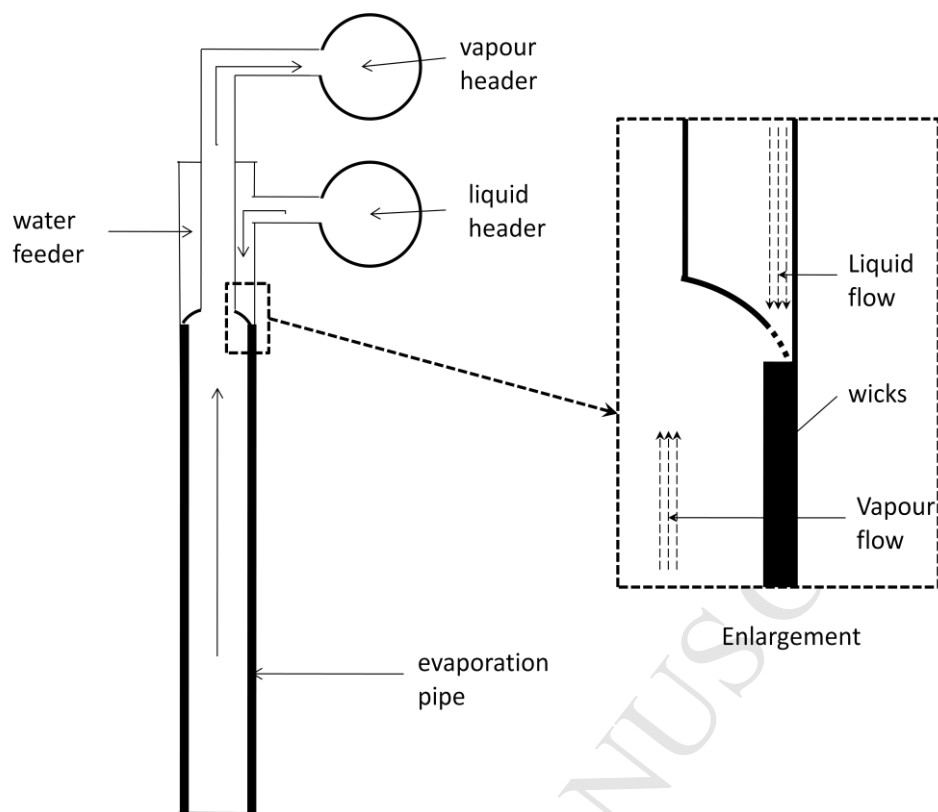


Fig. 2. Schematic of the connection of the headers and heat pipes via the water feeder

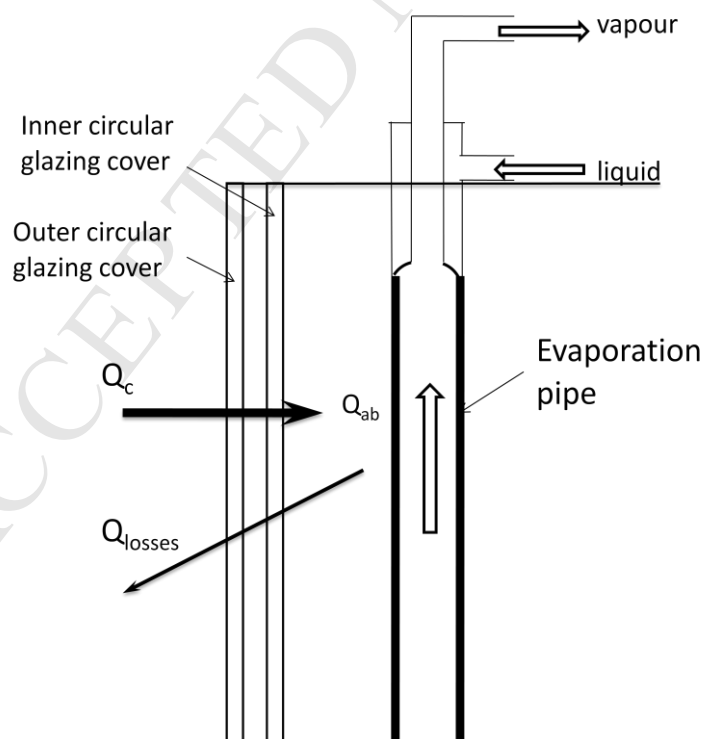


Fig. 3. Schematic of the heat transfer within the absorber area

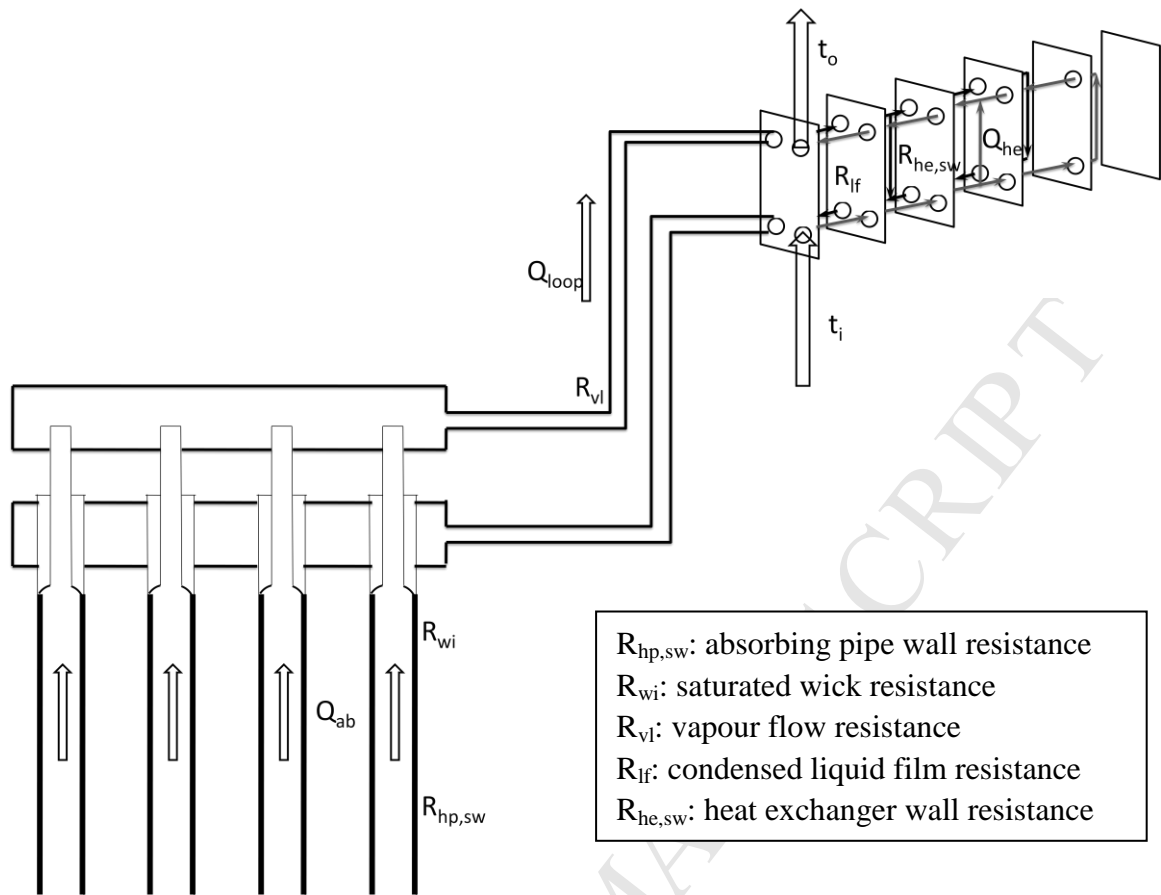


Fig. 4. Schematic of the heat transfer from absorbers to heat exchanger

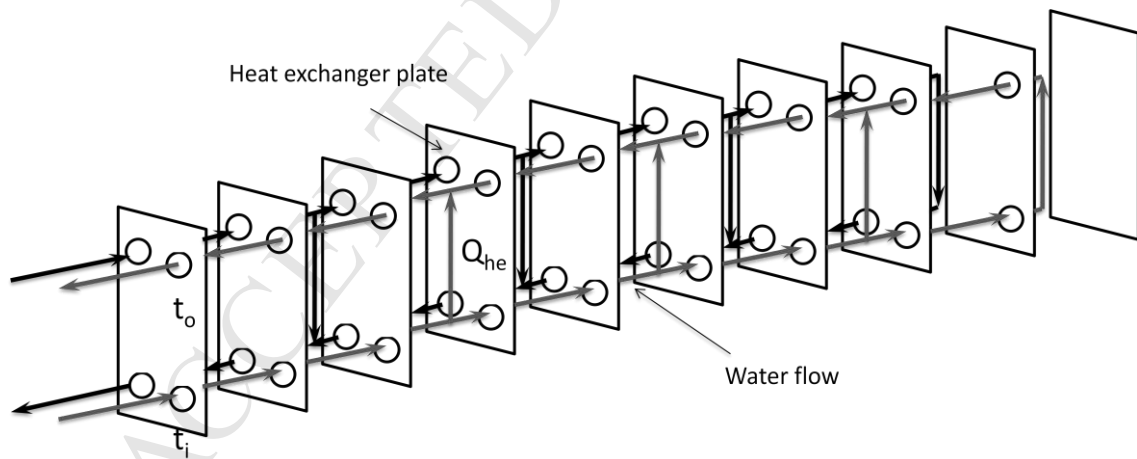
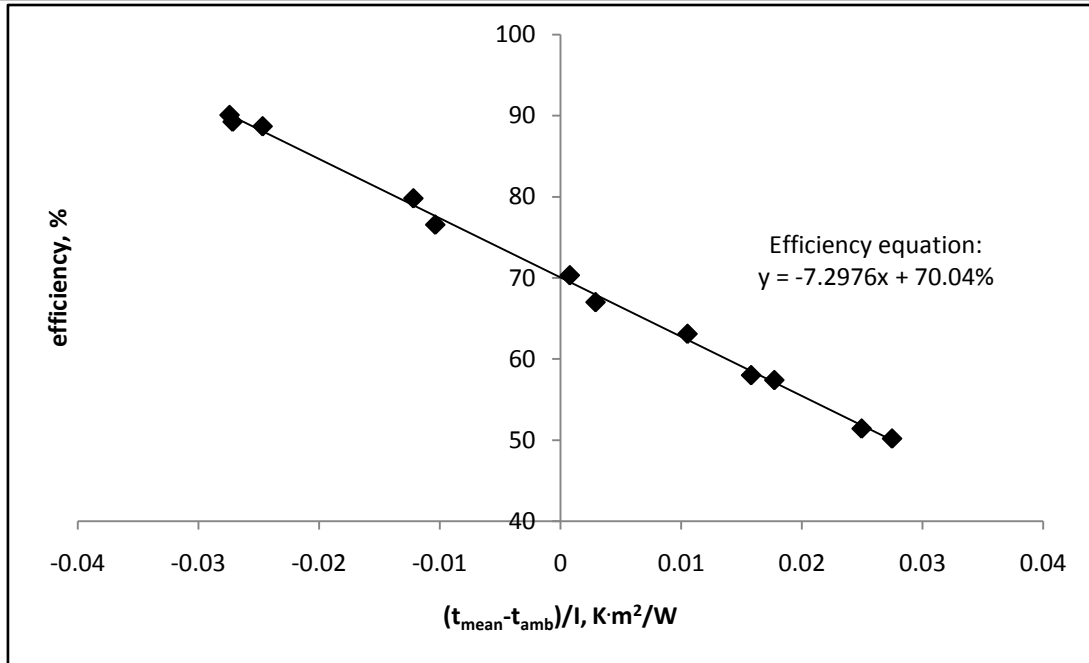
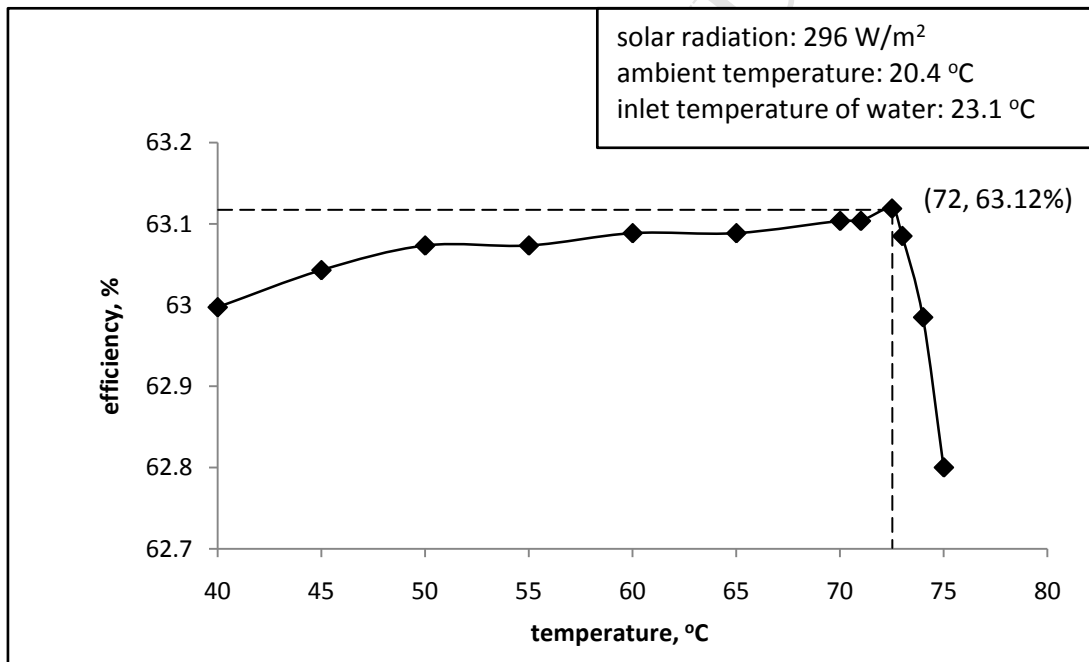
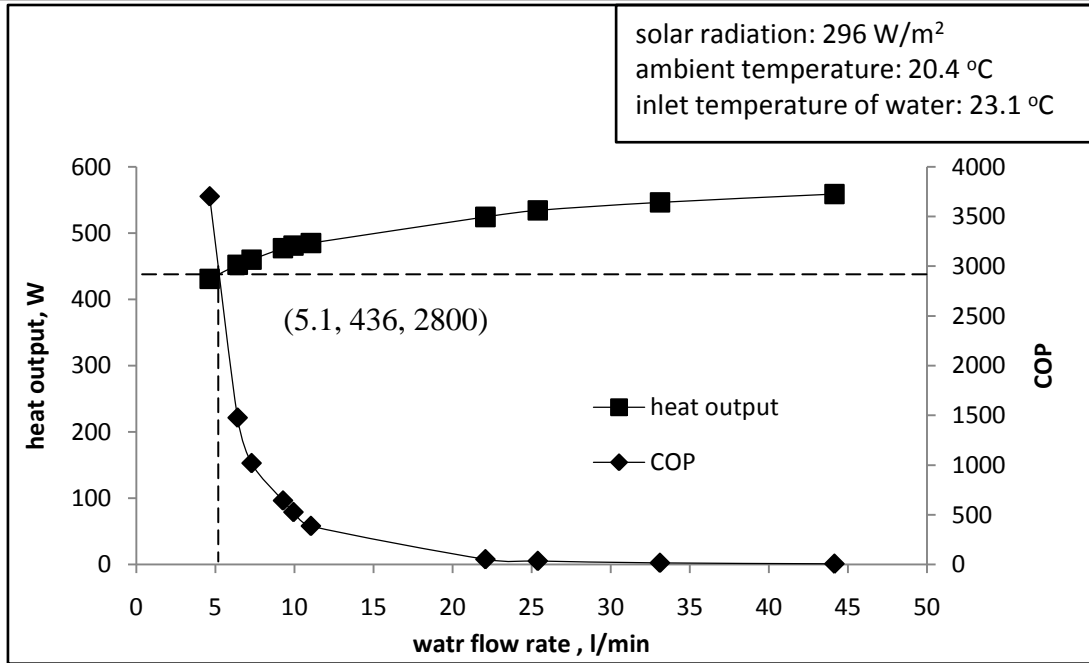
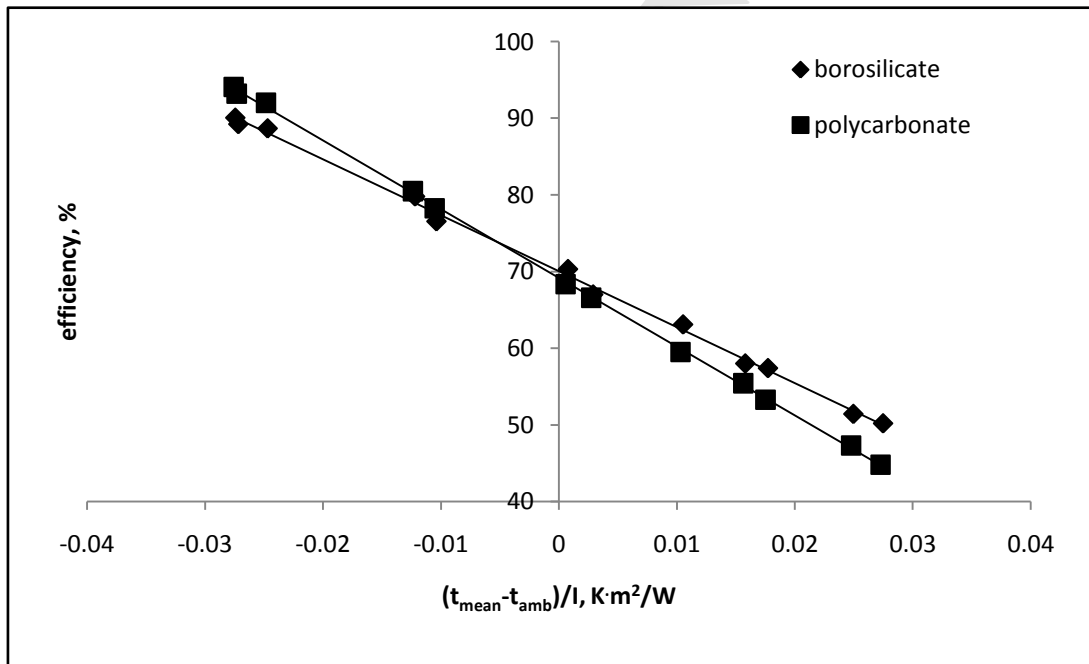


Fig. 5. Schematic of the heat transfer between condensed liquid and passing water within the heat exchanger

Fig. 6.  $\eta - (t_{\text{mean}} - t_{\text{amb}})/I$  relation (borosilicate glazing)Fig. 7.  $\eta$  .vs. operating temperature (borosilicate glazing)

Fig. 8.  $\eta$  vs. water flow rate (borosilicate glazing)Fig. 9.  $\eta - (t_{\text{mean}} - t_{\text{amb}})/I$  relation – for two types of the absorber glasses

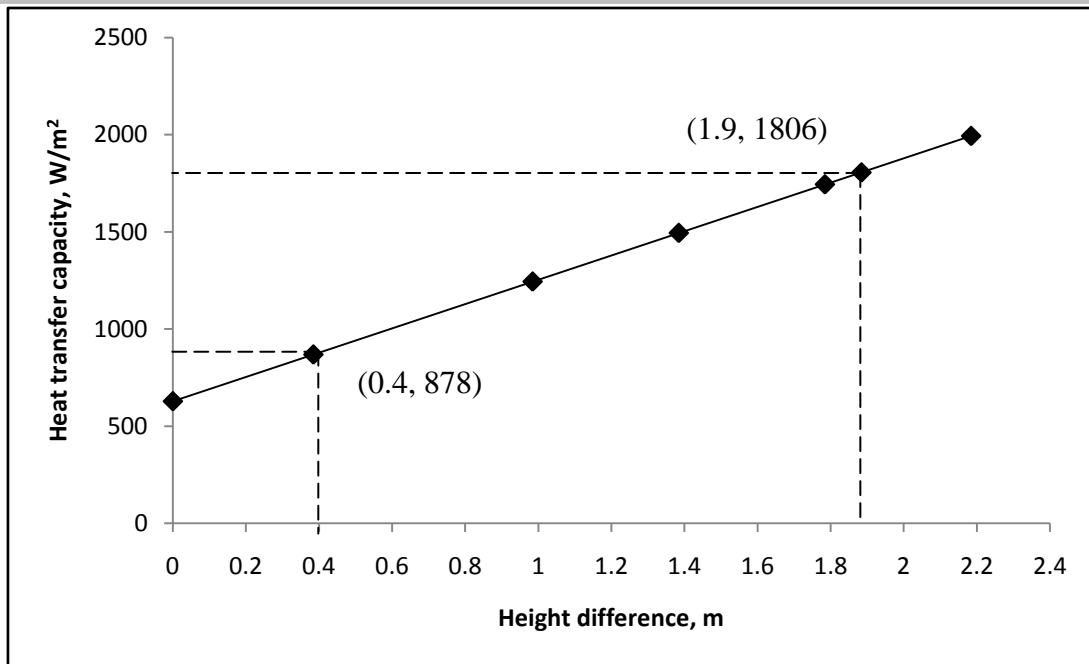


Fig. 10. Heat transfer capacity .vs. height difference between the top absorber and heat exchanger

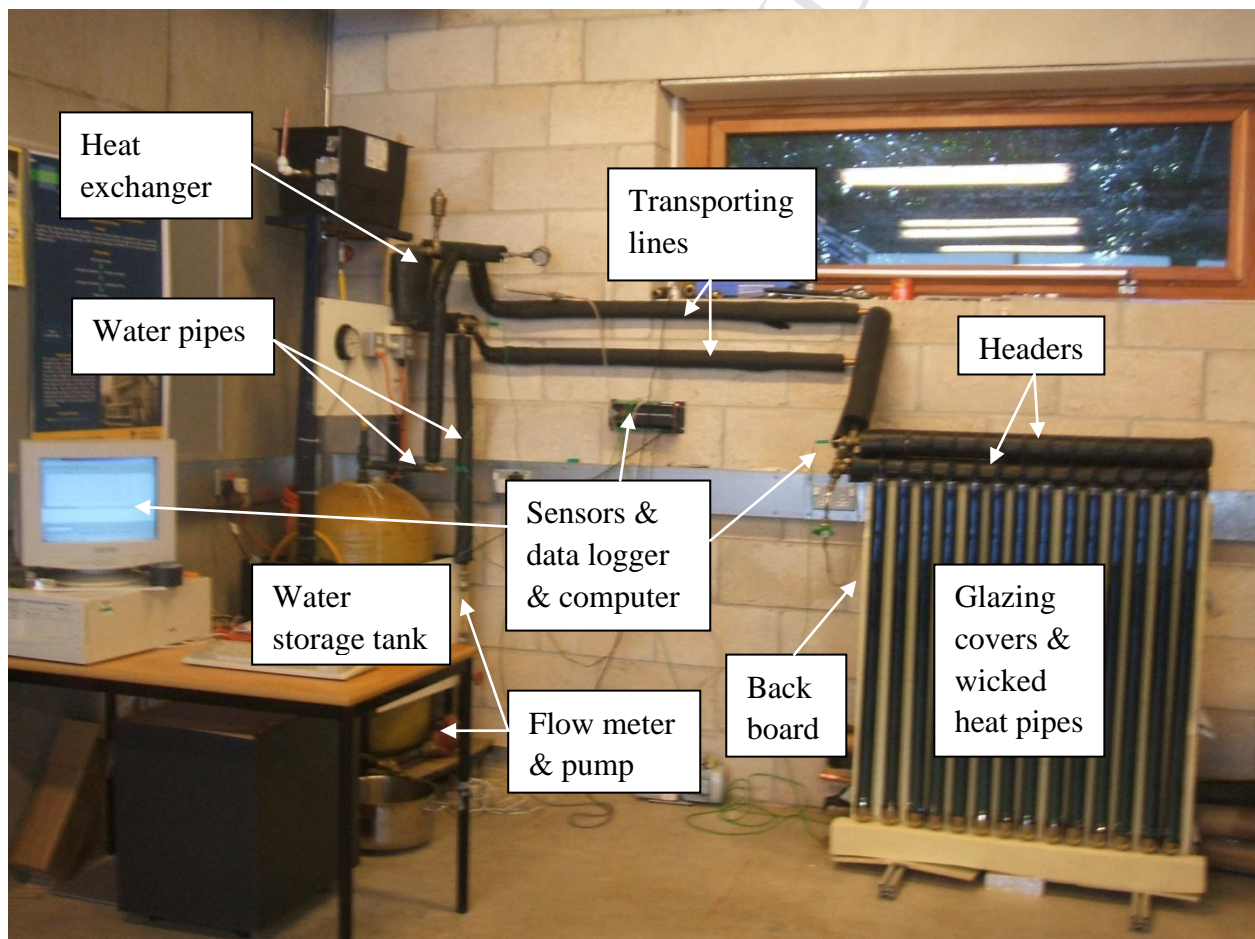


Fig. 11. Photograph of the prototype and its testing rig

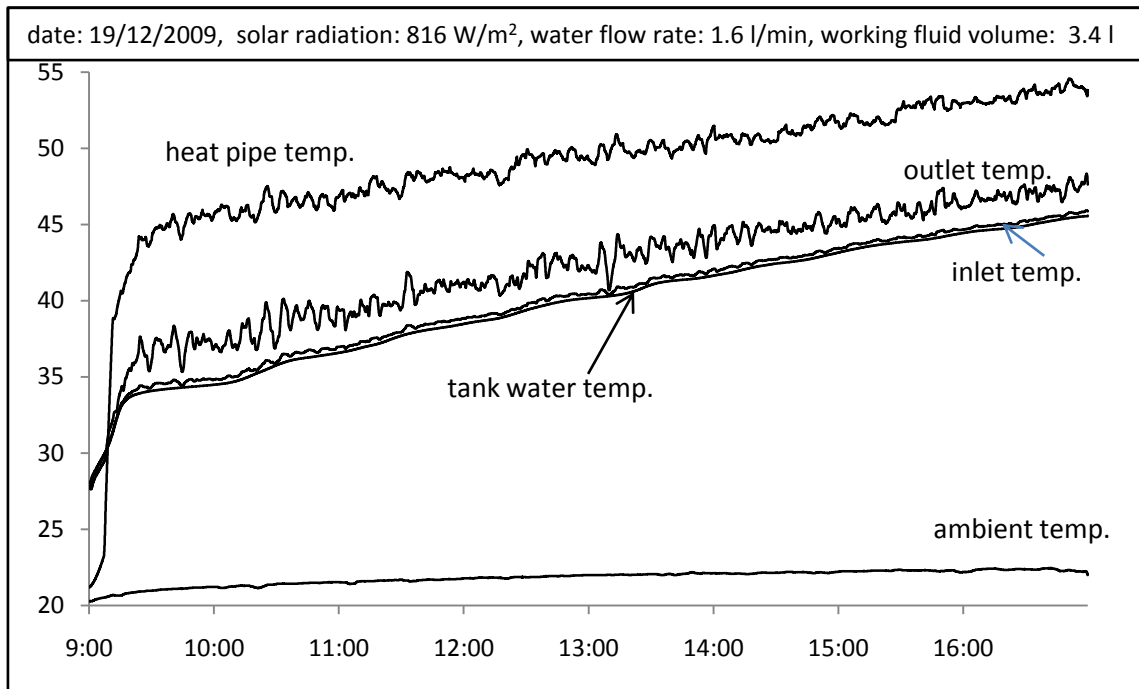


Fig. 12. Temperatures .vs. time

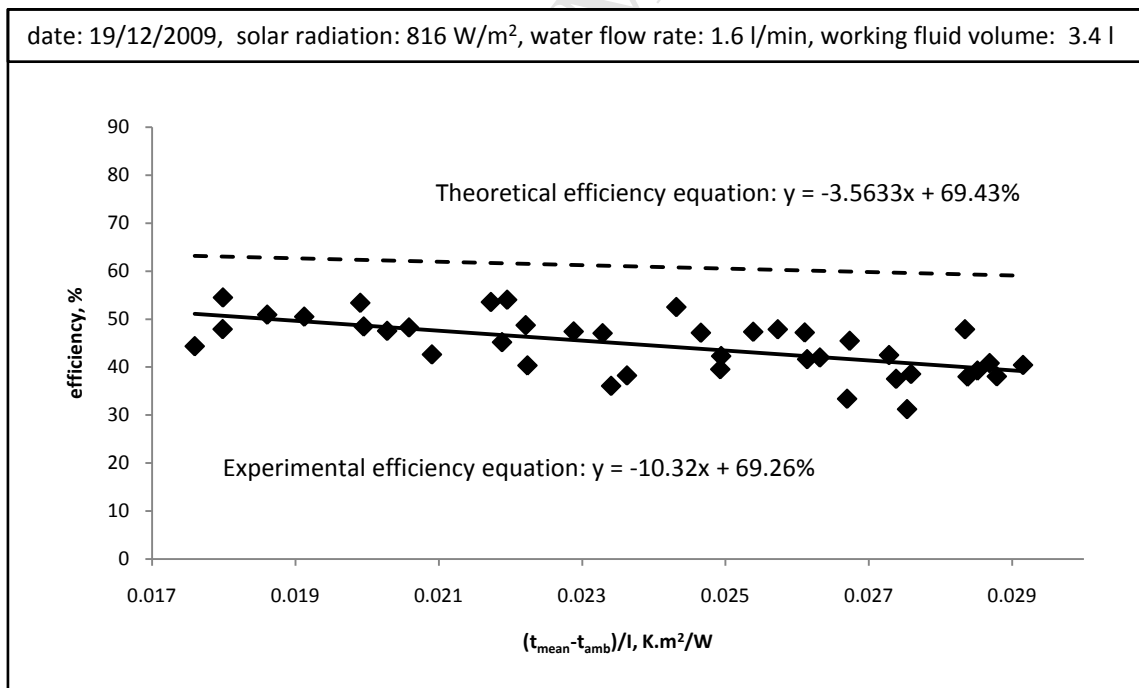


Fig. 13. Comparison of the theoretical and testing efficiencies

Table 1. Solar optical, thermal and geometric parameters of glazing covers and wall board

Glazing covers - borosilicate				
Outer circular glazing cover	Transmittance $\tau_{gc,o}$	0.93	Length $L_{gc,o}$ (m)	1.48
	Absorptivity $\alpha_{gc,o}$	0.03	Thickness $\delta_{gc,o}$ (m)	0.003
	Emissivity $\varepsilon_{gc,o}$	0.02	Thermal conductivity $\lambda_{gc,o}$ (W/m·K)	1.2
	Diameter $D_{gc,o}$ (m)	0.058	Number $N_{gc,o}$	44
Inner circular glazing cover	Transmittance $\tau_{gc,i}$	0.93	Length $L_{gc,i}$ (m)	1.48
	Absorptivity $\alpha_{gc,i}$	0.03	Thickness $\delta_{gc,i}$ (m)	0.003
	Emissivity $\varepsilon_{gc,i}$	0.02	Thermal conductivity $\lambda_{gc,i}$ (W/m·K)	1.2
	Diameter $D_{gc,i}$ (m)	0.047	Number $N_{gc,i}$	44
Glazing covers - polycarbonate				
Outer circular glazing cover	Transmittance $\tau_{gc,o}$	0.88	Length $L_{gc,o}$ (m)	1.48
	Absorptivity $\alpha_{gc,o}$	0.06	Thickness $\delta_{gc,o}$ (m)	0.003
	Emissivity $\varepsilon_{gc,o}$	0.82	Thermal conductivity $\lambda_{gc,o}$ (W/m·K)	0.2
	Diameter $D_{gc,o}$ (m)	0.058	Number $N_{gc,o}$	44
Inner circular glazing cover	Transmittance $\tau_{gc,i}$	0.88	Length $L_{gc,i}$ (m)	1.48
	Absorptivity $\alpha_{gc,i}$	0.06	Thickness $\delta_{gc,i}$ (m)	0.003
	Emissivity $\varepsilon_{gc,i}$	0.82	Thermal conductivity $\lambda_{gc,i}$ (W/m·K)	0.2
	Diameter $D_{gc,i}$ (m)	0.047	Number $N_{gc,i}$	44
Wall board – EPS with steel sheet attached back				
Length $L_{wb}$ (m)		3.04	Width $W_{wb}$ (m)	0.149
Height $H_{wb}$ (m)		1.48	Thermal conductivity of EPS $\lambda_{wb}$ (W/m·K)	0.039

Table 2. Characteristics of the absorber panel and wicked heat pipes

Absorbers – copper fins			
Transmittance $\tau_{ab}$	0.03	Thickness $\delta_{ab}$ (m)	0.0005
Absorptivity $\alpha_{ab}$	0.95	Thermal conductivity $\lambda_{ab}$ (W/m·K)	383.79
Emissivity $\varepsilon_{ab}$	0.1	Number $N_{ab}$	44
Area for one absorber $A_{ab}$ (m <sup>2</sup> )	0.069	Absorptivity of coating materials (nickel) $\alpha_c$	0.98
Evaporation pipes – copper			
Length of pipes $L_{hp}$ (m)	1.32	Diameter of vapour channel $D_v$ (m)	0.014
Outer diameter of pipes $D_{hp,o}$ (m)	0.0165	Inner diameter of pipes $D_{hp,i}$ (m)	0.0155
Number $N_{hp}$	44		
Two layers mesh screen wicks - copper			
Length $L_{wi}$ (m)	1.32	Diameter of pores $D_p$ (m)	0.00003855
Thickness of one layer $\delta_{wi}$ (m)	0.000375	Number of pores $N_p$	9158

Table 3. Properties of vapor header, vapor line and water tube

Vapour header – stainless steel			
Length $L_{vh}$ (m)	2.982	Inner diameter $D_{vh}$ (m)	0.086
Vapour line – cast iron			
Length $L_{vl}$ (m)	5	Inner diameter $D_{vl}$ (m)	0.048
Water pipes – cast iron			
Length $L_{wp}$ (m)	5	Inner diameter $D_{wp}$ (m)	0.02

Table 4. Specifications of heat exchanger configurations

Heat exchanger – stainless steel			
Length $L_{he}$ (m)	0.119	Plate thickness $\delta_{he}$ (m)	0.00024
Width $W_{he}$ (m)	0.3176	Plate thermal conductivity $\lambda_{he}$ (W/m·K)	16.28
Height $H_{he}$ (m)	0.289	Number of plate $N_{he}$	140

Table 5. Summary of external parameters and calculation results

Month	Solar radiation I (W/m <sup>2</sup> )	Ambient temp. t <sub>amb</sub> (°C)	Inlet temp. of water flow t <sub>i</sub> (°C)	Outlet temp. t <sub>o</sub> (°C)	Mean temp. t <sub>mean</sub> (°C)	(t <sub>mean</sub> -t <sub>amb</sub> )/I	Efficiency η (%)	Final temp. of the water in a 8-hour day-time operation (°C)
1	354	-2.94	2.2	3.1	2.5	0.0155	58	42.7
2	351	0.1	0.6	1.6	1	0.0025	67	47.2
3	323	6.1	2.2	3.3	2.6	-0.0108	77	51.2
4	319	14.3	5	6.3	5.5	-0.0277	89	61
5	265	20.4	12.6	13.7	13	-0.028	90	59.2
6	240	25.2	18.8	19.7	19.2	-0.0251	89	60.1
7	229	26.4	23.2	24	23.5	-0.0127	80	58.5
8	251	25	24.8	25.6	25.1	0.0004	70	58.9
9	296	20.4	23.1	23.9	23.4	0.0102	63	59.2
10	304	13.7	18.7	19.5	19	0.0174	57	52.7
11	292	4.8	12.5	13.1	12.7	0.0272	50	41.1
12	298	-0.5	6.6	7.3	6.9	0.0247	51	40.8

Table 6. Thermal and geometric parameters of the prototype system

Double glazing covers – borosilicate			
Transmittance $\tau_{gc}$	0.86	Length $L_{gc}$ (m)	1.02
Absorptivity $\alpha_{gc}$	0.06	Thickness $\delta_{gc}$ (m)	0.0055
Emissivity $\varepsilon_{gc}$	0.04	Thermal conductivity $\lambda_{gc}$ (W/m·K)	2.4
Outer diameter $D_{gc,o}$ (m)	0.058	Number $N_{gc}$	14
Inner diameter $D_{gc,i}$ (m)	0.047		
Absorbers – copper fins			
Transmittance $\tau_{ab}$	0.03	Thickness $\delta_{ab}$ (m)	0.0005
Absorptivity $\alpha_{ab}$	0.95	Thermal conductivity $\lambda_{ab}$ (W/m·K)	383.79
Emissivity $\varepsilon_{ab}$	0.1	Number $N_{ab}$	14
Total heat transfer area $A_{ab}$ (m <sup>2</sup> )	0.716	Absorptivity of coating materials (nickel) $\alpha_c$	0.98
Gross area (m <sup>2</sup> )	0.942		
Heat pipes – copper			
Length of pipes $L_{hp}$ (m)	1	Outer diameter of pipes $D_{hp,o}$ (m)	0.016
Number $N_{hp}$	14	Diameter of vapour channel $D_v$ (m)	0.014
Inner diameter of pipes $D_{hp,i}$ (m)	0.0155	Volume of working fluid (l)	3.4
Two layers mesh screen wicks - copper			
Length $L_{wi}$ (m)	1	Diameter of pores $D_p$ (m)	0.00003855
Number of pores $N_p$	9158	Thickness of one layer $\delta_{wi}$ (m)	0.000375
Vapour header (liquid header) – copper			
Length $L_{vh}$ (m)	0.982	Diameter $D_{vh}$ (m)	0.04
Vapour line (liquid line) – copper			
Length $L_{vl}$ (m)	2.5	Diameter $D_{vl}$ (m)	0.02
Heat exchanger – stainless steel			
Length $L_{he}$ (m)	0.119	Plate thickness $\delta_{he}$ (m)	0.00024
Width $W_{he}$ (m)	0.3176	Plate thermal conductivity $\lambda_{he}$ (W/m·K)	16.28
Height $H_{he}$ (m)	0.289	Number of plate $N_{he}$	20
Water pipes – copper			
Length $L_{wp}$ (m)	5	Diameter $D_{wp}$ (m)	0.02
Water tank			
Volume $V_{tank}$ (m <sup>3</sup> )	0.18		